Mutation Research 756 (2013) 213–223

Contents lists available at ScienceDirect

Mutation Research/Genetic Toxicology and Environmental Mutagenesis

journal homepage: www.elsevier.com/locate/gentox
Community address: www.elsevier.com/locate/mutres

Track structure based modelling of chromosome aberrations after photon and alpha-particle irradiation

Werner Friedland*, Pavel Kundrát

Helmholtz Zentrum München – German Research Center for Environmental Health, Institute of Radiation Protection, Ingolstädter Landstr. 1, 85764 Neuherberg, Germany

ARTICLE INFO

Article history:
Received 17 June 2013
Accepted 18 June 2013
Available online 28 June 2013

Keywords:
Radiation track structure
DNA damage repair
Chromosome aberrations
Monte Carlo simulation
Mathematical modelling

ABSTRACT

A computational model of radiation-induced chromosome aberrations in human cells within the PARTRAC Monte Carlo simulation framework is presented. The model starts from radiation-induced DNA damage assessed by overlapping radiation track structures with multi-scale DNA and chromatin models, ranging from DNA double-helix in atomic resolution to chromatin fibre loops, heterochromatic and euchromatic regions, and chromosome territories. The repair of DNA double-strand breaks via non-homologous end-joining is followed. Initial spatial distribution and complexity, diffusive motion, enzymatic processing, synapsis and ligation of individual DNA ends from the breaks are simulated. To enable scoring of different chromosome aberration types resulting from improper joining of DNA fragments, the repair module has been complemented by tracking the chromosome origin of the ligated fragments and the positions of centromeres. The modelled motion of DNA ends has sub-diffusive characteristics and corresponds to measured chromatin mobility within time-scales of a few hours. The calculated formation of dicentrics after photon and α-particle irradiation in human fibroblasts is compared to experimental data (Cornforth et al., 2002, Radiat Res 158, 43). The predicted yields of dicentrics overestimate the measurements by factors of five for γ-rays and two for α-particle irradiation. Nevertheless, the observed relative dependence on radiation dose is correctly reproduced. Calculated yields and size distributions of other aberration types are discussed. The present work represents a first mechanistic approach to chromosome aberrations and their kinetics, combining full track structure simulations with detailed models of chromatin and accounting for the kinetics of DNA repair.

1. Introduction

Ionizing radiation is capable of inducing various types of damage to cellular DNA, of which the most critical ones are DNA double-strand breaks (DSB). To preserve chromosome and genome integrity, cells are equipped with dedicated repair pathways. The dominant pathway of DSB repair in eukaryotic cells is non-homologous end-joining (NHEJ), active throughout the cell cycle [1]. Homologous recombination (HR) contributes in the S/G2 phases when a sister chromatid is available as a repair template [1]. Incorrect repair may lead to the formation of chromosome aberrations [2–4], which have been implicated in radiation-induced cell killing [5–9] as well as in carcinogenesis [10,11].

Several alternative theories on the origin of chromosome aberrations (CA) have been proposed, reviewed in [7,12–14]: In the one-hit (or damage–nondamage interaction) theory, a single radiation-induced DSB is sufficient to initiate a reaction with undamaged DNA that may lead to CA, resembling the mechanism involved in HR repair of DSB. In the exchange theory, the initial chromosome lesions are unstable and decay with time but may also interact with another lesion and produce a CA. In the breakage-and-reunion theory, CA follow from incorrect joining of a chromosome free end with another end, resembling the NHEJ pathway of DSB repair. The breakage-and-reunion theory is nowadays the favoured theory of CA origin for cells in the G0/G1 phase on which this paper is focused; the one-hit mechanism likely contributes in the S/G2 phase [12,13].

Mathematical modelling represents a valuable tool complementing experimental research. It helps obtain quantitative insights and test alternative hypotheses on mechanisms underlying the studied phenomena. Modelling also provides the means to extrapolate the experimental results to conditions that can hardly be assessed directly, e.g. measured CA yields to low and very low doses that are of particular interest for risk assessments.

Motivated by these aims, a number of models for radiation-induced CA have been proposed. They differ in the level of details considered on the structures of radiation tracks, DNA and chromatin, and correspond to diverse CA origin theories. Instead of

* Corresponding author. Tel.: +49 89 3187 2767; fax: +49 89 3187 3363.
E-mail address: friedland@helmholtz-muenchen.de (W. Friedland).

1383-5718/$ – see front matter © 2013 Elsevier B.V. All rights reserved.
http://dx.doi.org/10.1016/j.mrgentox.2013.06.013

following the course of break processing and mobility (chromatin dynamics), only their final outcome in terms of joining correct or incorrect chromatin fragments is considered, with diverse assumptions on the distance-dependence of the misrejoining probability between chromosome break ends. Edwards et al. [6,15] considered DSB distributed randomly over the nucleus, for high-LET radiation taking into account radial distributions of ionization events. The misrejoining probability decreased with the DSB distance according to an inverse power law; an option to include a time-dependent factor as in the exchange theory of CA was discussed, too. Sachs et al. used a semi-analytical approach and presented considerations on chromatin dynamics governing the distance-dependent misrejoining [17]. Later, Sachs et al. [18] simulated chromosome territories as cylinders in which DSB induced by low-LET radiation were distributed randomly; the misrejoining probability exponentially decreased with the DSB distance. Cucinotta et al. [19] studied, in addition to the pairwise interaction, also the one-hit mechanism in which enzymatic processing of a single break may lead to simple exchanges. Ballarini et al. [7,8,20,21] modelled interphase chromosomes by a random walk of 200 nm boxes. Chromosome free ends resulted from complex DSB ('cluster lesions'), whose yield was taken from track structure simulations or treated as an adjustable parameter. For low-LET radiation the lesions were distributed randomly, whereas a track core and penumbra model was used for high-LET radiation. The interaction probability was uniform up to an adjustable maximal distance of chromosome ends. Holley et al. [22] modelled chromosomes as random polymers inside spherical territories. DSB were assessed by track structure simulations accounting for both direct and indirect (water radical-mediated) effects. A fraction of DSB was allowed to undergo pairwise misrejoining, with a Gaussian distance-dependence. Kreth et al. [23] constructed chromosome territories by a sequence of spherical chromatin domains, distributed DSB for low-LET radiation randomly, and described the DSB interaction probability by an inverse power law. A similar spherical domain model of chromatin structure was employed by Eidelman et al. [24]. In their approach, CA formation required a contact of two DSB-containing domains, assessed by their dynamic chromatin model, and subsequent DSB interaction, described by an adjustable contact-exchange probability. Alternatively, each DSB produced a chromosome break, and breaks interacted throughout the whole nucleus independently of their distance. Ponomarev et al. [25] used a random walk polymer representation of chromosomes, distributed DSB according to amorphous radiation track structures, and assumed a Gaussian distance-dependent misrejoining probability.

Although differing in the particular assumptions on the distance-dependent misrejoining probability, the existing CA models have in common that they employ only a phenomenological description of repair outcome. Despite the connection between improper DSB repair by NHEJ and aberration induction in G0/G1 cells [26], the CA models lack a detailed link to chromatin dynamics and DSB repair.

On the other hand, NHEJ models have been proposed recently [27–30] that exploit the tremendous amount of experimental knowledge accumulated in the last two or three decades on the underlying processes of the NHEJ pathway: Following DSB induction, rapid local chromatin decondensation occurs which leads to activation of ATM and further chromatin remodelling with histone removal and nucleosome repositioning [1,31,32]. The Ku70/80 heterodimer, a rather small protein with a ring structure, is commonly considered to be the first major player in NHEJ. Ku is a highly abundant protein that binds to most ends as they become accessible [1]. When the nucleosomes surrounding the damage site are released, the DNA end with attached Ku recruits DNA-PKcs [1]. The synapsis of two DNA ends proceeds via dimerization of DNA-PKcs and their auto-phosphorylation. Conformational changes in DNA-PKcs make the DNA ends accessible to other NHEJ players, in particular Artemis that is involved in end processing and XRCC4-Ligase IV that performs the final ligation steps [1]. In addition to the above-described classical NHEJ, some DSB are repaired by alternative pathways not involving DNA-PK [1]. Finally, higher-order chromatin structures and the 'epigenetic code' are restored, presumably not always perfectly, thus potentially leading to 'epimutations' [33].

The NHEJ models [27–30] account for the major steps in biochemical processing of DSB and their kinetics. The attachment and action of repair enzymes are often expressed using the law of mass action as a system of kinetic equations (set of ordinary differential equations). There are two limiting aspects to these approaches: First, continuous models with reaction rate equations require that the numbers of DSB and repair enzymes are relatively large. For typical radiation doses leading to small DSB numbers, discrete stochastic models are more appropriate [28]. Second, the spatial aspects of NHEJ, on which the experimental information is unfortunately by far not as mature as the knowledge on the enzymes involved, are commonly neglected in the modelling, although they critically influence both the kinetics and the outcome of DSB joining. For instance, opening of the DSB is needed already for the Ku ring to attach to the DNA end and presumably even more for larger enzymes such as DNA-PKcs. Importantly, spatial aspects govern the ratio of proper vs. improper joining as well as the formation of CA. According to the breakage-and-reunion theory, only breaks (more precisely, broken ends) that come close together during the course of repair may get ligated and form aberrations.

This drawback of insufficient representation of spatial aspects in repair models has been removed by the NHEJ simulation module [34–36] in the PARTRAC biophysical modelling suite [37]. The simulations start by assessing DNA damage by overlapping space- and time-dependent radiation track structures with detailed models of DNA and chromatin structure. Namely, individual energy deposits to DNA and surrounding water molecules, production of reactive species, their diffusion and mutual reactions, and attacks to DNA are simulated. Multiple levels of chromatin structure are considered, from the DNA double-helix and nucleosomes to chromatin fibres, domains and territories that represent human cell nuclei in the interphase. An atomic DNA model enables predicting radiation quality-dependent complexity of DNA damage. The NHEJ module [34–36] follows in addition to the temporal development (i.e. the course of enzymatic processing) also the spatial movement of DNA ends based on the following hypotheses: First, following the chromatin remodelling step, the DSB 'opens' and forms a chromatin break, i.e. the break ends get mobile. Their mobility is limited by attachment sites where the fibre is anchored to the nuclear scaffold but not by tethering to the other end. Note that, on the contrary, other DSB repair and CA models treat DSB as a single entity, i.e. assume that the two free ends of any DSB are steadily held in proximity to each other, and CA result from (unspecified) pairwise interaction of DSB, not from joining wrong DNA ends. The second underlying hypothesis extends the first one by assuming that the experimentally observed mobility of chromatin regions can be applied to these DSB-induced ends as well. Within the repair simulation, the movement of broken ends and their processing by NHEJ enzymes are modelled simultaneously by stochastic Monte Carlo methods. These two processes together decide on which end pairs become ligated, i.e. these two aspects together govern the repair outcome, including the formation of CA.

In this paper, we extend the PARTRAC NHEJ module to CA simulations and thereby provide a link between models of repair processes and of CA. This extension consists of the following issues: First, data on the positions of centromeres have been implemented into the chromatin structure module. Second, the chromatin model has been extended to distinguish between regions of different chromatin densities (condensed heterochromatin and more relaxed,

transcriptionally active euchromatin). Third, the NHEJ module has been supplemented by tracking the history of each joining event that involves DNA fragments from different chromosomes or intra-chromosomal incorrect joining (inversions or ring formations). After the end of the repair simulation, these history files on chromosome exchange events are analyzed with respect to different types of CA, in particular the involvement of centromeres (e.g. dicentrics and centric vs. acentric rings). Importantly, even the yields of small DNA fragments and rings are simulated, which are hardly detectable in cytogenetic experiments but likely produced especially by high-LET radiation.

The PARTRAC approach represents a bottom-up, 'ab initio' simulation that combines radiation track structures with DNA and chromatin models to assess the induced damage, and explicitly models its spatially and temporally dependent repair. In this paper, we focus on model assumptions, methods and possibilities to test specific hypotheses on DSB repair and CA formation, including the effects of radiation quality, chromatin structure, and mobility of DNA ends. As a first benchmark of the model, results of simulations of CA induction after γ-ray and α-particle irradiation are shown and compared with corresponding experimental data gathered by Cornforth et al. [38]. We do not aim at providing simulations with parameter adjustments to reproduce the measured CA data since the calculation includes no 'free' parameter. Instead, the deviations between calculation and experiments will initiate careful revision of the basic model assumption in view of the most recent state of knowledge in this field. This task which goes beyond the scope of this paper will be accompanied by thorough parameter testing with respect to the resulting model predictions on radiation quality and dose-dependent DSB repair dynamics, CA induction and chromatin mobility issues.

2. Materials and methods

2.1. Experimental data used

Cornforth et al. [38] measured chromosome aberrations in AG1522 primary human skin fibroblasts upon irradiation by γ-rays or α-particles. Cell cultures were kept under the conditions of density-inhibited growth, i.e. were essentially quiescent, with less than 1% cells in the S-phase of their cycle. The cells were irradiated by γ-rays from a ^{137}Cs source (dose rate of 31.2 Gy/h) or by α-particles from a ^{238}Pu source (2.3 Gy/min; with 3.5 MeV mean energy and 116 keV/μm ionization density of alphas traversing cell nuclei). 1 h post irradiation, the cells were released from density inhibition by re-plating at lower densities. Using a 3–4 h blocking with mitosis inhibitor Colcemid, metaphase collections were made at intervals ranging for γ rays from 30 to 42 h and for alphas from 25 to 60 h after the release from density inhibition. Metaphase spreads known to be at the first mitosis post irradiation were analyzed using Giemsa staining. The scoring of CA included dicentrics, centric and acentric rings, and interstitial and terminal deletions. Further details on the methods can be found in [38].

2.2. Calculation of track structures

To model the irradiations used in the reported experiments [38], track structures of 662 keV photons from ^{137}Cs decay and α-particles with 4.0 MeV initial energy, yielding the average energy of 3.5 MeV in the middle of the cell nuclei (hereafter referred to as 3.5 MeV α-particles), were calculated with PARTRAC. Particle tracks were calculated in a cuboidal world region with 22 μm × 12 μm × 8 μm side lengths; energy depositions were scored in a concentric cuboidal target region of 20 μm × 11.2 μm × 6.4 μm surrounding an ellipsoidal volume with these values as x-, y- and z-axis lengths that represented a human fibroblast nucleus. The model of chromatin structure within the nucleus is described below. The radiation source was modelled by a 22 μm × 12 μm rectangular plane located at $z = -4$ μm normal to that axis. Primary particles were started randomly from the source approximately perpendicularly to its surface, strictly speaking with an angle φ between the surface normal and the track direction possessing a uniform distribution of cos φ in the interval [0.95,1] in order to avoid geometrical alignment with chromatin structures. The first photon interaction was mirrored into the target region. Scattered photons and α-particles that had left the target region were not further considered; for secondary electrons, periodic boundary conditions were imposed corresponding to full equilibrium conditions, i.e. electrons leaving the target region were assumed to enter on the opposite side with the same movement direction and velocity.

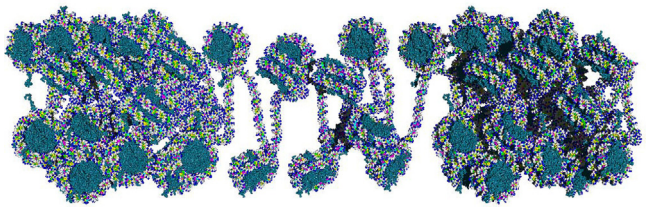

Fig. 1. POV-Ray™ ray-tracer representation of two basic linear elements of heterochromatic DNA with a basic linear element of euchromatic DNA in-between. Blue: phosphate group atoms; white: sugar group atoms; green, yellow, red, violet: atoms of adenine, guanine, cytosine and thymine bases, respectively; turquoise: histone atoms.

Individual interactions of the primary photons, α-particles, and of secondary electrons down to 10 eV energy were simulated step-by-step by Monte Carlo methods, representing the stochastic nature of radiation interactions with matter. The contributions of individual interaction processes (such as ionizations and excitations) are given by the corresponding cross sections. For photons, tracks were simulated in a hypothetical homogeneous medium that accounts for the abundances of diverse chemical elements in cell nuclei; the cross sections for the elements were taken from the EPDL data base [39] and weighted accordingly. For electrons and α-particles, inelastic interaction cross sections in liquid water according to the work by Dingfelder [40,41] were used.

DNA damage due to direct effects was determined by superimposing the distributions of energy deposition events with a multi-scale DNA target model, which is described in detail below. Events outside the union of atoms of DNA constituents and histones were assumed to produce, within the pre-chemical stage, reactive species in the water surrounding the target volume. During the subsequent chemical stage, the diffusion of these reactive species and their interaction with each other were traced step-by-step with parameters described in Kreipl et al. [42]. Moreover, interactions of •OH radicals with sugar moieties and bases of the DNA were determined and scored as DNA damage due to indirect effects [43]. In addition to •OH consumption due to interactions with other reactive species and DNA constituents, the action of further •OH-scavenging molecules in the cell nucleus was taken into account by a decay rate of 4×10^8 s^{-1} (i.e. •OH lifetime of 2.5 ns). Further details on the simulations and discussion of the assumptions and parameters are reviewed in [37].

2.3. Multi-scale DNA model

In this work, an extension of the recent DNA model in PARTRAC [37] has been used that distinguishes between hetero- and euchromatic regions of the cell nucleus. The model will be described in full detail elsewhere. Briefly, it is based on two sets of five types of stackable chromatin fibre elements, one linear and four 90°-bent ones. Each of these boxes contains an atomic representation of the DNA and histones inside, which enables scoring the complexity of damage induced by diverse radiation types. The boxes used in this work possess a 40 nm edge length; the size of the boxes has been reduced from 50 nm used previously [37] in order to allow building the human genome within the same nuclear volume but using to a greater part the less condensed chromatin structures. The first set of boxes describes condensed chromatin of heterochromatic DNA with 24 nucleosomes (5065 bp) in the linear element and 16 nucleosomes (about 3310 bp) in the bent elements. The second set represents euchromatic DNA, with 10 and 6 nucleosomes (2065 and 1220 bp) in the linear and bent elements, respectively. Fig. 1 shows a basic linear euchromatic DNA element placed between two heterochromatic ones. Seamless connection between all elements of both sets is realized by placing a single nucleosome at the same position on the border between adjacent elements and by avoiding any further intersection of DNA or nucleosomes with this interface.

The chromatin in a human fibroblast nucleus with an ellipsoidal shape is modelled as a randomized walk on the 40 nm grid, representing a loop structure of the chromatin fibre around centres of spherical chromatin domains (SCD) of 1 Mbp size, cf. [37]. Chromosome territories of the 46 chromosomes in human fibroblast nuclei are generated by a connected sequence of SCDs; the SCD centres are taken from a corresponding realization of a human fibroblast nucleus by the SCD model [44]. The model respects the differences in sizes and preferred positions among the chromosomes. Within each SCD, chromatin fibre elements at minimum distance to SCD centres are considered to represent nuclear attachment sites for the adjacent loops. Within the repair model described below, these attachment sites serve as anchorage points for the movement of DNA ends produced by DSB; the locations of these attachment sites are fixed throughout the whole repair process. Totally, the fibroblast nucleus comprises 6×10^9 base pairs within about 2×10^6 basic elements. In Fig. 2, a ray-tracer representation of the fibroblast nucleus model is shown, with chromosomes highlighted in different colours.

The distribution of hetero- and euchromatic regions within the nucleus has been taken from an isochore map of human chromosomes [45]. The isochore map divides the genome into nearly 3200 segments of 5 isochore families, denoted by L1, L2, H1,

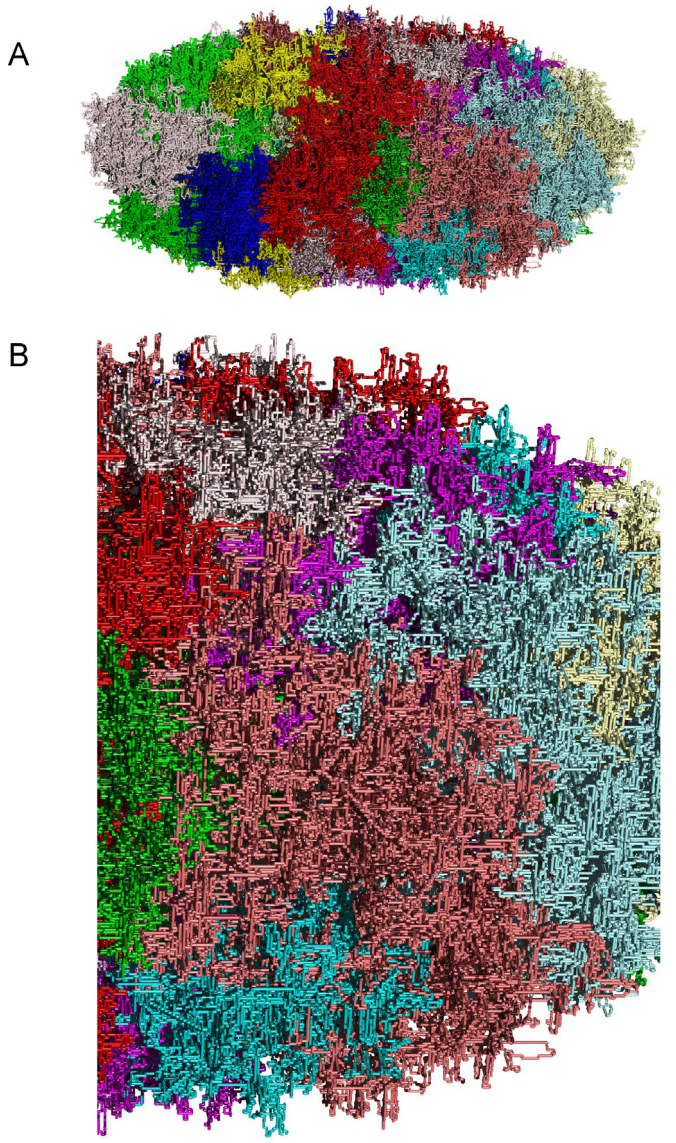

Fig. 2. POV-Ray™ ray-tracer representation of the fibroblast nucleus model (Panel A) and a zoomed view of a section (Panel B). Different chromosomes are shown in different colours. Basic elements (cubes of 40 nm side length) are represented by tubes with 32 nm diameter corresponding to the chromatin fibre.

H2 and H3, with increasing cytosine-guanine (CG) levels of <37%, 37–41%, 41–46%, 46–53% and >53%, respectively. Isochore families correlate not only with gene density but also with chromatin structure in interphase nuclei [45]. The 'genome core' of families H2 and H3 comprises more than half of the genes within 15% of the genome, whereas the 'genome desert' (families L1, L2 and H1) consists of large expanses with low or extremely low gene densities [45].

In the chromatin model of this work, the correlation between CG-rich regions of the genome and euchromatin has been taken into account by adopting a CG fraction of 55% in the basic euchromatic elements and of 34% in basic heterochromatic elements. Individual segments belonging to the isochore families L1, L2, H1, H2 and H3 were mapped to chromatin fibres consisting of 100%, 80%, 60%, 30% and 0% heterochromatic and a complementary fraction of euchromatic elements (40 nm boxes), respectively. In the heterogeneous families L2, H1 and H2, hetero- vs. euchromatic boxes have been ordered at random; the L1 and H3 families contain boxes of one type only (heterochromatic or euchromatic, respectively). Gaps in the isochore data set at centromeric regions have been filled by heterochromatin (L1) and in the chromosome arms with euchromatin (H3). Positions of centromeres have been taken from chromosome arm data [46].

2.4. Calculation of the initial DNA damage

The assumptions on the process of DNA damage induction by radiation that are used in PARTRAC have been reviewed recently [37]. In this work, the parameters from [35] have been used for the calculation of the initial DNA damage (and repair, see below). Briefly, DNA strand breaks from direct effects are assumed to occur with a probability that increases linearly from 0 at 5 eV to 1 at 60 eV energy deposit in a single sugar-phosphate group. Strand breaks from indirect effects are assumed to arise from 65% of interactions between •OH radicals and the deoxyribose moiety of DNA. Whenever at least two strand breaks (resulting either from direct or indirect effects) are found within 10 bp on the opposite DNA strands, a DSB is scored. Furthermore, a conversion of 1% of single-strand breaks into DSB is assumed. Base lesions result from direct energy depositions to or interaction of •OH radicals with atoms of DNA bases, and contribute to the complexity of DSB. Only a fraction of these lesions is assumed to slow-down the DNA repair process. This repair-retarding fraction is determined from base damage due to direct effects with the probability increasing linearly from 0 at 0 eV to 1 at 60 eV deposited energy, and due to indirect effects in 25% of the •OH interactions with bases [35].

2.5. Calculation of DNA repair

The previously published module describing DSB repair via NHEJ [34–36] has been used in this work. The parameter selection according to [35] has been guided by the adequate reproduction of photon and ion induced initial DNA damage and its rejoining; later model refinements [36] have not been included here due to computational expensiveness issues. Briefly, the stochastic model of DSB repair by NHEJ pathway in PARTRAC tracks separately the processing of the two DNA ends from each DSB. The following characteristics of DNA ends obtained by the initial DNA damage calculation are taken into account: First, geometric and genomic position within the nucleus and the chromosome is considered, here including information on whether the end is located in hetero- or euchromatic region. Second, the length of the chromatin fibre from the DNA end to the next nuclear attachment site or to the next DSB (whatever comes first) is scored. Third, DNA damage complexity is assessed; to this end, nearby strand breaks or repair-retarding base lesions are counted until an undamaged sequence of 20 bp is found [37].

Contrary to other NHEJ models [27–30], the basic entity followed by the PARTRAC NHEJ model is not the DSB itself but the individual DNA ends produced by the DSB. This concept enables one to account not only for temporal development of DNA ends (attachment of repair enzymes and processing of the ends), but also for the spatial aspects, which are crucial for misrejoining and CA formation. Before the actual repair simulation starts, individual DNA ends are classified into clean DNA ends without nearby damage and dirty DNA ends carrying nearby single-strand break(s) and/or repair-retarding base lesion(s). Dirty ends are assumed to need additional processing during the NHEJ repair process.

2.5.1. Time course of NHEJ

The time course of the NHEJ repair scheme used in this work is presented in Fig. 3. The individual processes are described by first-order kinetics and modelled stochastically, i.e. the actual period required for a given processing step of a given DNA end is allowed to fluctuate around the time constant (inversed rate) of the process. The adopted time constants (in seconds) are listed in Fig. 3. For processes during the pre-synaptic phase, the time constants were derived [34] from experiments on enzyme kinetics [47,48]. Further parameters were adapted so that model calculations reasonably agree with experimentally determined repair kinetics [49]. Rates (time constants) of the individual processing steps have been assumed constant, independent of the DSB numbers and also the states of the other DNA ends. This is justified as the doses and hence DSB numbers analyzed in this paper are rather low, while repair enzymes such as Ku and DNA-PKcs are highly abundant in the nucleus [30,50] and/or can be reused in the processing of another DSB, e.g. LigIV-XRCC4 being re-adenylated by XLF-Cernunnos for the next ligation event [51].

Simultaneously with the progression of the repair steps, diffusive motion of individual DNA ends is considered. There are theoretical reasons [52] as well as experimental data [53–55] indicating that the mobility of DNA ends in the dense, dynamic network of chromatin fibres is sub-diffusive, i.e. that the corresponding diffusion coefficient decreases with time. For the sake of simplicity, however, we have kept our previous concept [34] of semi-free diffusion (confined by nuclear attachment sites) with two diffusion coefficients, describing a higher mobility of free ends before synapsis and a lower mobility of paired ends in the synaptic complex. Namely, the mobility of DNA ends is simulated with a diffusion coefficient of 170 nm^2/s during the first phase of NHEJ, and by a parallel movement of DNA ends that had formed the synaptic complex with a tenfold reduced diffusion coefficient [56]. Furthermore, this step-by-step random walk process is limited (confined) by the nuclear volume and the chromatin fibre lengths from the fixed nuclear attachment sites or by the fibre length for short fragments generated by two DSB on the same loop. To account for the spatial effects of chromatin remodelling triggered by the DSB induction [1,32], the (geometric) fibre length from the attachment site to the free DNA end is allowed to gradually increase with time, with a length increment of 5 nm per 1000 s. As shown in the Results, this mobility concept effectively provides an apparent diffusion of DSB (ends) that agrees with data on chromatin dynamics and telomere mobility.

The temporal development, i.e. DSB processing, starts in the present NHEJ model with a chromatin remodelling and DNA end mobilization step that opens the gap between the two DNA ends from the DSB and makes them accessible to repair proteins (step 1 in Fig. 3) [1,32]. The first NHEJ enzyme that is attached to the DNA end is

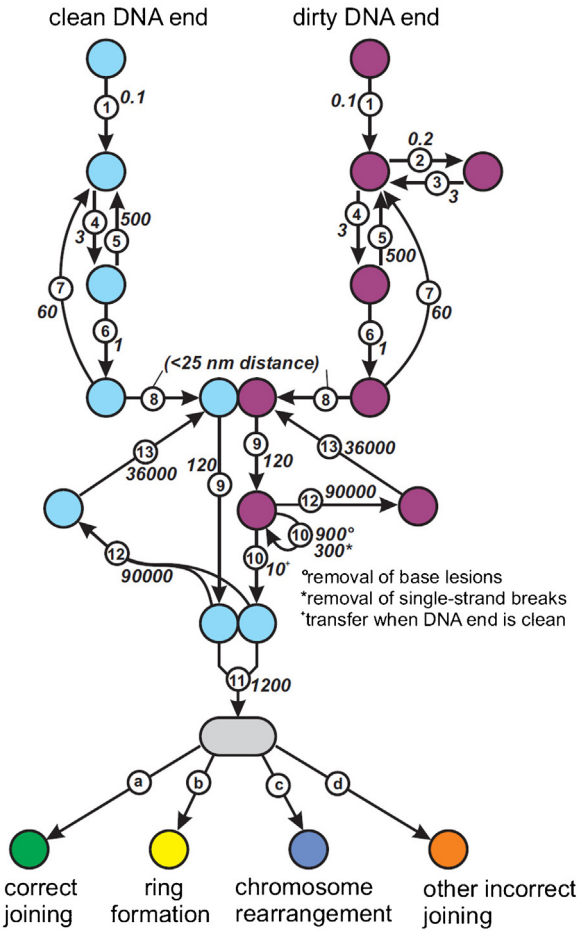

Fig. 3. Scheme of the temporal development in the DNA repair and chromosome aberration model for joining of a clean DNA end (without nearby lesions; blue) and a dirty DNA end (carrying nearby lesions; violet). Transfers between states are modelled in first order kinetics; numbers in italic denote their time constants in seconds.

Ku70/80 (step 4) [1,57]. For dirty DNA ends, potential recruitment of other proteins is considered that inhibit Ku70/80 attachment (step 2) until they are removed again (step 3). In step 6, DNA-PK complex is formed after binding of the catalytic subunit DNA-PKcs to Ku70/Ku80 at the DNA end [1,57]; corresponding enzyme dissociation (steps 5 and 7) is represented, too. A synaptic complex is formed (step 8) between two DNA ends (clean or dirty) with attached DNA-PK complexes [1,57]. In the simulation, synapsis occurs when two DNA ends with DNA-PK are separated by less than 25 nm [36]. The spatial vicinity of the DNA ends in synapsis is conserved during further processing steps. The two DNA-PK complexes cross-phosphorylate each other and further NHEJ repair enzymes are attached and activated (step 9) [1,57]. For dirty ends, nearby single-strand breaks and base damages are removed in a 'lesion-by-lesion' way (step 10) until the DNA end is clean and rejoinable. Finally, the two DNA ends are ligated (step 11). By this, one DSB is removed, i.e. it is no longer detected within the experimental DSB repair kinetics protocol, e.g. using pulsed-field gel electrophoresis [49]; note however that repair foci may persist for some time post end-joining. Temporal blocking of final ligation within the post-synaptic phase (step 12) with a release step (step 13) is considered, too. The joined DNA ends are classified into (a) correctly rejoined DNA ends, (b) formation of rings, i.e. ligation of the two ends of a DNA fragment, (c) interchromosomal misrejoining, i.e. ligation of DNA ends from different chromosomes, and (d) other forms of misrejoined DNA ends within a single chromosome (intrachromosomal misrejoining). DNA fragments shorter than 25 bp are assumed to be intrinsically unrejoinable [34], as DNA-PK does not exhibit its kinase activity when attached to such short fragments [58]; similarly, fragment length of at least 15 bp was required for Ku attachment in another NHEJ modelling work [28].

2.5.2. Spatial aspects of NHEJ

A simplified scheme of the DNA repair and CA model in PARTRAC highlighting its spatial aspects is provided in Fig. 4. The DNA and chromatin structure model uses 40 nm cubes as basic building blocks, visualized in this 2D projection by dashed squares: square #1 with a straight chromatin segment, #2 with a bent one, and square #3 including a projection of two straight elements that appear as if they

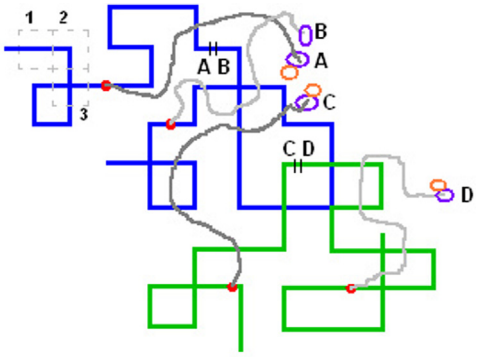

Fig. 4. Schematic illustration of spatial aspects of the DNA repair and chromosome aberration model in PARTRAC (see text).

crossed each other. From these building blocks, chromatin loops are constructed (blue and green lines, being parts of different chromosomes). In the depicted region, radiation insult has induced two DSB, denoted by two short vertical lines. After a chromatin remodelling and DSB opening step, PARTRAC follows separately the individual DNA ends formed by a DSB. Chromatin dynamics is a crucial component that underlies aberration formation. In PARTRAC, the chromatin dynamics itself is not modelled explicitly, but only its impact on the movement of DNA ends is considered, i.e. no dynamic model of the chromatin structure is employed, but only the DNA ends are tracked. The mobility of the DNA ends is modelled stochastically as a semi-free diffusion. Yet the segments (curly grey lines) are kept attached at nuclear attachment sites (red points). The diffusive motion of the DNA ends is limited by the segment lengths (from the attachment site to the DNA end), which, as discussed above, increase with time due to chromatin remodelling. Simultaneously, the DNA ends are processed by the repair enzymes involved in NHEJ (depicted by rings attached to the ends). Also this processing is simulated stochastically, so that some DNA ends proceed through the NHEJ faster than others. As a result, not all breaks are correctly rejoined, for a number of reasons. First, the two ends formed by a DSB may diffuse relatively far apart before their joining might have occurred (DNA ends labelled by C and D). Second, the two ends might have stayed close to each other (DNA ends labelled A and B) but might have proceeded to different stages of the NHEJ, so that they cannot join readily: the A end has both Ku70/80 (violet ring) and DNA-PKcs (orange ring) attached, but the B end is missing DNA-PKcs, so that they cannot form a synaptic complex and ligation cannot take place. If by chance another end with both Ku70/80 and DNA-PKcs comes close enough to the A end, as is shown with the C end, these two may get joined, although the DNA molecules actually belong to different chromosomes. Obviously, the chance for such two ends to come close to each other is higher for ends originally in proximity than for those originally far away from each other. Note also that the type of chromosome aberration produced by this misrejoining depends on the fate of other DNA ends formed by the given radiation dose, including the original partners of the A and C ends, i.e. ends B and D, which at the time point captured by this illustration continue searching for a potential ligation partner via diffusive motion.

2.6. Dose dependent repair calculation

In the analyzed irradiation regimes, individual particle tracks induce DNA damage including DSB independently of other tracks; synergistic effects of multiple tracks at the level of damage induction occur only at extremely high doses or dose rates [43]. To save computational time, the expensive DNA damage simulation has been thus performed only once in this work. The damage simulation has been divided into 2000 runs with at least 0.895 MeV energy deposition (0.1 Gy radiation dose) for γ-ray irradiation and 1000 runs with exactly 6 α-particles. The total energy deposits amounted to 2201 MeV for γ-rays and 4295 MeV for α-particles, giving average doses D_{av} of 0.123 Gy and 0.480 Gy per run, respectively. The dose ranges of 0–6.1 Gy for γ-rays and 0–2.2 Gy for α-particles used in the CA experiments [38] has been covered by grouping the corresponding numbers of damage simulation runs: The DNA damage simulated in groups of, e.g. four subsequent runs was allocated into 2000/4 = 500 cells exposed to doses of ∼0.5 Gy for γ-rays and 1000/4 = 250 cells with ∼2 Gy for α-particles. Thus, the simulation of DNA repair kinetics started for all doses with the same data set of DSB, however, synapsis and final joining has been restricted to pairs of DNA ends within the same cell.

2.7. Analysis of chromosome aberrations

DNA end joining events up to 4 days post irradiation have been considered in the CA analysis. The actual choice of the time point is not very critical as just a few joining events occur in the late NHEJ phases 1 day post irradiation or later (not shown). The previously used scoring of joining processes of DNA fragments [34] has been complemented with data on chromosome number, fragment size and with information on whether centromeres are included. Immediately following each correct or incorrect

joining event, the composition of the respective fragments stored within the simulation has been updated. This includes fragments containing DNA from different chromosomes. In the final classification step, fragments have been checked for the presence of centromeres. To enable a refined comparison of simulated results with cytogenetic data, the code also includes an option to specify the smallest fragment sizes and other detection limits of the experiments.

3. Results

The simulation of initial DNA damage resulted in 13,374 DNA ends for ^{137}Cs γ-irradiation, corresponding to a DSB yield of 4.5 DSB per Gy and Gbp (about 27 DSB per cell per Gy). For 3.5 MeV α-particles, 62,550 DNA ends were obtained, corresponding to a DSB yield of 10.9 DSB per Gy and Gbp (65 DSB per cell per Gy). Note that these seemingly high yields for high-LET radiation are caused by having included short DNA fragments that are hardly detectable experimentally in fragmentation studies; the experimental underestimation of DSB yields by high-LET radiation has been discussed previously [59].

3.1. Outcome of NHEJ repair: rejoining vs. misrejoining of DNA ends

Radiation induces DSB somewhat more frequently in euchromatic than in heterochromatic regions, as heterochromatic DNA is protected against indirect radiation effects by histones that effectively scavenge radicals (results will be shown elsewhere). Globally speaking, however, γ-ray induced DSB are randomly distributed over the nucleus, with relatively large distances between DSB pairs. As a result, although the DNA ends are mobile, the chance of finding a 'wrong' partner is rather low, and the majority of breaks are correctly rejoined (resituated). The correctly rejoined fraction slightly decreases with radiation dose, and for the studied 0–8 Gy dose range corresponds to 85–95% (Fig. 5A). Intra- and interchromosomal misrejoining and ring formation slightly increase with increasing dose, but stay below 2–7% of events.

The 3.5 MeV α-particles, on the other hand, possess high ionizing density (LET about 115 keV/μm), and induce streaks of DSB along their tracks. Individual tracks are randomly distributed over the nucleus; the mean number of tracks per cell is proportional to the applied dose. Although single tracks are well separated, the DSB formed within a single track are relatively close to each other, which enhances the chance that incorrect DNA ends diffuse into close proximity and get misrejoined. In the simulations, only about 30% of DNA ends are correctly rejoined, whereas slightly above 30% ends undergo intrachromosomal and about 15% of ends even interchromosomal misrejoining, and about 20% participate in rings (Fig. 5B). Also the fraction of very short fragments that are assumed intrinsically unrejoinable is larger than for the γ-rays (about 5% vs. less than 1%, respectively). Note that contrary to the case of γ rays, the fate of DNA ends induced by α-particles is practically independent of radiation dose, indicating that single-particle effects dominate over intertrack ones.

We have previously shown that the PARTRAC NHEJ simulations agree with experimental data on DSB repair kinetics for low- and high-LET radiation [34–36]. The well-known biphasic repair kinetics, when the majority of DSB are joined within less than 1 h but a small DSB fraction requires repair times of several hours [49], is in the model attributed to the fact that dirty DNA ends from complex DSB require additional enzymatic processing steps [34–36]. In agreement with DSB repair kinetics data [49], even after 1 day repair there is a fraction of not yet rejoined (but rejoinable) DNA ends. For ^{137}Cs γ and 3.5 MeV α-irradiation studied in this work, this fraction amounts to about 5% and 8% of DNA ends, respectively (not shown), and reduces to about 2–3% of DNA ends when the repair is followed for 4 days; this unrejoined fraction is almost

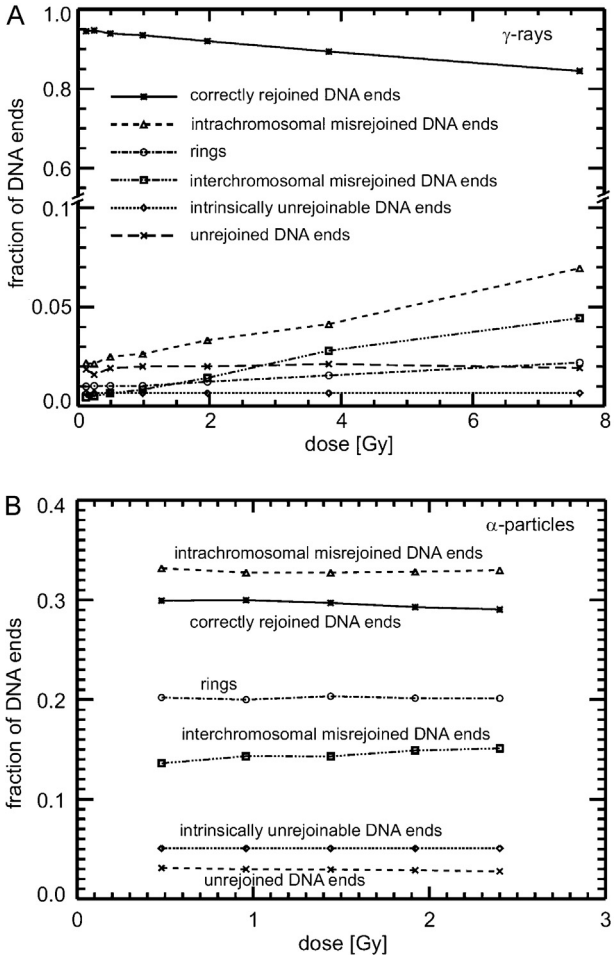

Fig. 5. States of DNA ends after 96 h repair. Dose-dependent fractions of DNA end states due to (A) ^{137}Cs γ-ray and (B) 3.5 MeV α-particle irradiation. Lines are drawn to guide the eyes only.

dose-independent (Fig. 5). These ratios are comparable with the yields of terminal deletions reported in cytogenetic experiments, which amount to 1–3% for γ-ray and 10% for α-particle irradiation, respectively [38].

3.2. Chromatin mobility and distance-dependent misrejoining

Fig. 6 shows, for α-particles at 2.4 Gy dose, the distribution of the original geometric distances of DNA ends that were incorrectly joined within a single chromosome (intrachromosomal misrejoining, dashed line) or between different chromosomes (interchromosomal misrejoining, solid line). As expected, the probability of joining is high for ends originally in proximity and rapidly decreases with increasing distance. For both intra- and interchromosomal misrejoining, the decrease is approximately exponential, as seen from the almost linear behaviour in the logarithmic plot. For intrachromosomal misrejoining, 50% of these events happen within the distance of 80 nm, and 90% within 410 nm. For interchromosomal events, the median misrejoining distance is 280 nm, and the 90% percentile corresponds to 830 nm. For rings (these are not included in the intrachromosomal misrejoining above), the 50% and 90% percentiles are 15 and 150 nm, respectively (results not shown). However, the ring formation is likely overestimated, as the present simulations assume that even the ends of rather short fragments are freely diffusive so that they may come close together and form small rings, which neglects the rigidity of the DNA molecule and chromatin fibres. Also note that the difference between

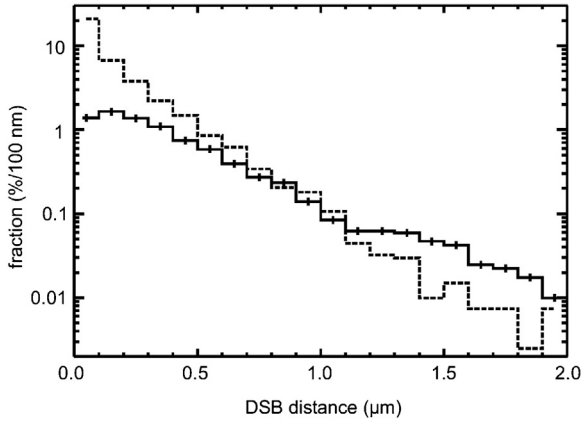

Fig. 6. Distribution of original distances between DNA ends that have participated in incorrect joining within a chromosome (intrachromosomal misrejoining, dashed line) and between different chromosomes (interchromosomal misrejoining, solid line). Calculated results for 2.4 Gy α-particle irradiation, normalized to the overall percentage of DNA ends participating in these misrejoining events as shown in Fig. 5.

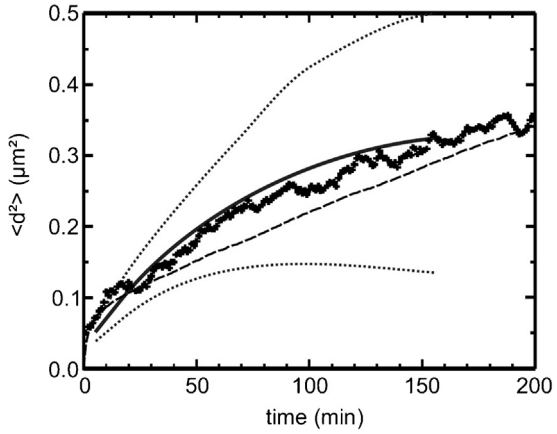

Fig. 7. Apparent sub-diffusive motion of DNA ends and chromatin. The calculated mean squared displacement $\langle d^2 \rangle$ in 2D projection along the z-axis according to either the distances between pairs of DNA ends (crosses) or the positions of individual DNA ends (dashed line) induced by 2.4 Gy α-particle irradiation are compared with relative motion of telomere pairs [54]. The reported mean values and error bars from an ensemble of 20–40 telomere trajectories measured by fluorescence microscopy in U2OS osteosarcoma cells [54] are marked by the solid and dotted lines, respectively, capturing their temporal development.

intra- and interchromosome misrejoining distributions could be traced to the fact that for a given DNA end, other ends induced within the same chromosome are on average closer than DNA ends formed on other chromosomes.

The mean squared displacement of DNA ends, plotted in Fig. 7 over an interval of more than 3 h post irradiation, reaches about 0.3 μm^2. Fig. 7 also shows that the mean squared displacement (and hence also the apparent diffusion coefficient) predicted by the present simulations reasonably agree with the data on telomere mobility [54] which is in turn comparable with the mobility of undamaged as well as damaged chromatin regions [32,54].

3.3. Dose-dependent yields of chromosome aberrations

The simulated dose-dependent yields of different types of CA after γ-ray and α-particle irradiation are presented in Fig. 8. In Panel A, the predicted yields of joined DNA fragments from different chromosomes including one centromere (monocentrics) and no centromere (acentrics) are shown as a function of dose for γ-rays and α-particles. The dose-dependence is almost linear

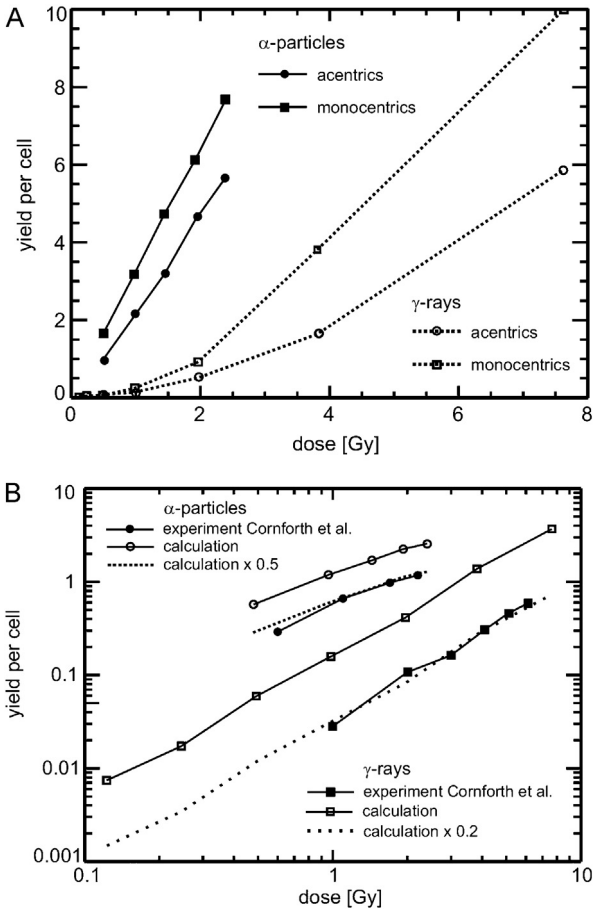

Fig. 8. Dose-dependent yields of chromosomal aberrations. (A) Calculated yields of acentrics and monocentrics (chromosome exchange aberrations without centromere and with a single centromere) after ^{137}Cs γ-ray (dotted lines) and 3.5 MeV α-particle irradiation (solid lines). (B) Calculated yields of dicentrics (chromosome exchange aberrations with two centromeres, open symbols) compared to experimental results by Cornforth et al. [38] (filled symbols) due to ^{137}Cs γ-ray (squares) and 3.5 MeV α-particle irradiation (circles). Dotted lines give calculated results multiplied by 0.2 for γ- and 0.5 for α-particle irradiation. Lines connecting the calculated or measured data points are drawn to guide the eyes only.

for α-particles and linear-quadratic for γ-rays. For both radiation types, monocentrics turned out to be more frequent than acentrics. In Fig. 8B, the dose-dependent simulation results are presented and compared to experimental data by Cornforth et al. [38]. The PARTRAC predictions exceed the measured data by factors of about 5 for γ-rays and about 2 for α-particles, almost independent of dose. This means that although overestimating the absolute yields of dicentrics, the simulations do reproduce the relative dependence on dose. Graphically, this is expressed by almost parallel curves in the log-log scale. Indeed, multiplying the simulated results by ad-hoc factors of 0.2 for γ-rays and 0.5 for α-particles (dotted lines in Fig. 8B) would bring the scaled results into agreement with the data. Similar adjustments to a single data point are often made in CA models that contain fit parameters such as misrejoining probabilities, cf. [25]. Since the present simulation is free of parameter adjustment due to its 'ab initio' character we address later issues that may have caused this systematic overestimation of the dicentrics data by the simulations (see Discussion). Note that a part of this discrepancy may be explained by the difference in scoring: In the simulations, dicentrics are formed by joining of two chromosome fragments that both carry a centromere (centric fragments), with or without additional acentric fragments (i.e. fragments from single chromosomes without centromeres). In the

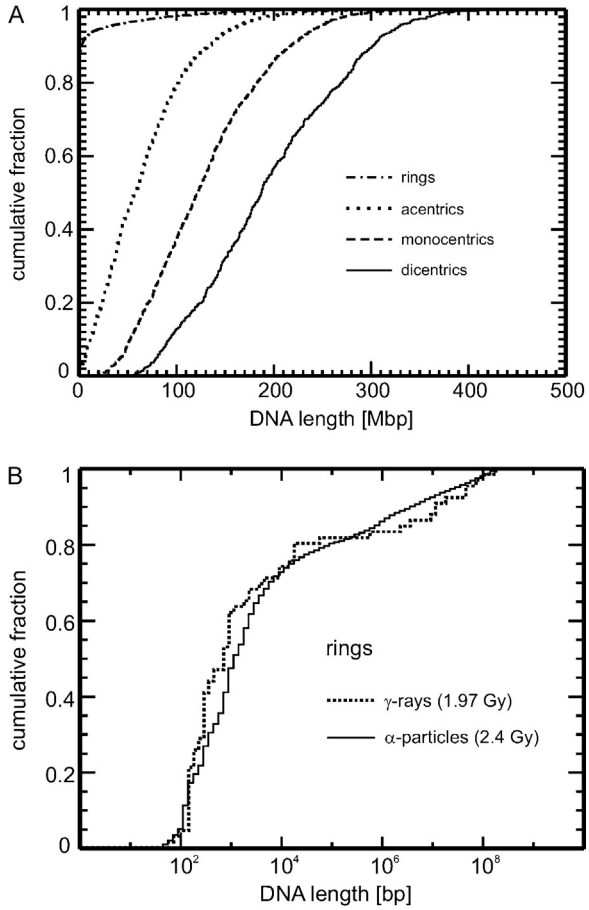

Fig. 9. Calculated cumulative size distribution of rings and chromosomal exchange aberrations. (A) Size distributions of rings (dash-dotted line), acentrics (dotted line), monocentrics (dashed line) and dicentrics (solid line) in the megabasepair range due to 3.5 MeV α-particle irradiation with 2.4 Gy. (B) Size distributions of rings over the whole size range due to ^{137}Cs γ-ray irradiation with 1.97 Gy (dashed line) and 3.5 MeV α-particle irradiation with 2.4 Gy (solid line).

experiments, however, dicentrics were scored only when chromosomes with two centromeres were found associated to an acentric fragment [38]. Rarely, joining of three or more centric fragments may occur; these events are not included among dicentrics here.

3.4. Size distributions of joined fragments and aberrant chromosomes

The present NHEJ and CA simulations naturally provide also the information on size distributions of fragments joined and the final products of joining. In Fig. 9A, simulated cumulative distributions of the sizes of dicentrics, monocentrics, acentrics and rings after 2.4 Gy α-particle irradiation are presented. The distribution for rings is also presented in Fig. 9B on an extended logarithmic length scale including the result after 1.97 Gy γ-ray irradiation. The ring size distributions for these two irradiations are very similar, with the majority of simulated rings quite short, <10 kbp, and only about 5% rings longer than 10–20 Mbp; note however that rings are formed by less than 3% of DNA ends induced by γ-radiation but by more than 20% of α-particle-induced ends (Fig. 5). Acentrics, monocentrics and especially dicentrics are significantly longer; the predicted median sizes for 2.4 Gy α-particle irradiation correspond to about 45, 120 and 190 Mbp, respectively (Fig. 9A).

Fig. 10 shows, for α-particle irradiation with 2.4 Gy, the predicted size distribution of centric fragments in dicentrics (solid line). For comparison, the size distribution of acentric fragments

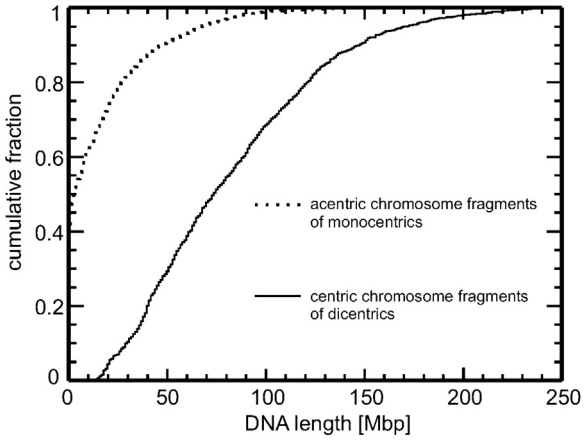

Fig. 10. Calculated cumulative size distribution of fragments in chromosomal exchange aberrations. Acentric chromosomal fragments in monocentrics (dotted line) and centric chromosomal fragments in dicentrics (solid line) due to 3.5 MeV α-particle irradiation with 2.4 Gy.

in monocentrics also is shown (dotted line). Centric fragments in monocentrics possess practically the same size distribution as the acentric ones (not shown). Note the large size differences among fragments in different types of CA. For instance, about 50% of acentric fragments in monocentrics but only 2% of centric fragments in dicentrics are shorter than 10 Mbp. These results show that having included in the simulations also short fragments not detectable in the experiments has not affected the simulated dicentrics yields, as only very few centric fragments are predicted below the detection limit for Giemsa staining, estimated as 15 Mbp [7].

4. Discussion

The PARTRAC biophysical family of codes and its CA module represent to our knowledge the first detailed mechanistic, bottom-up approach to CA modelling that accounts for full radiation track structure, multiple levels of DNA and chromatin organization in cell nucleus, and the temporal and spatial dynamics of DSB repair. The PARTRAC track structure module follows in an event-by-event manner all individual interactions of the primary particle as well as all secondary particles and their interactions. Most CA modelling approaches focus on low-LET radiation [15–17,23,24] or use a simplified description of amorphous tracks (radial dose distributions) only [8,25]. Accounting for full track structures and for spatially correlated energy deposition events is necessary not only for simulating the damage complexity, but also for assessing the yields of very short DNA fragments that either remain unrejoined or lead to small rings. Such short fragments have been predicted by PARTRAC [59] and recently considered also by Ponomarev et al. [25].

The DNA and chromatin structure modules of PARTRAC represent atomic DNA and chromatin fibre as well as its higher order structures with loops, chromatin domains, hetero- and euchromatic regions and chromosome territories. Some other CA models have used similar random-walk structures. However, they have not traced the full atomic structure of the DNA and histones, but used significantly larger objects as their basic building blocks, namely 2 kbp blocks [25], 200 nm cubes [8], or 1 Mbp (~500 nm) chromatin domains [23,24].

The DNA damage module in PARTRAC explicitly takes into account radiation damage through both direct and indirect mechanisms, i.e. via direct energy deposition to the DNA and via attacks of reactive species produced in water radiolysis. DSB are scored as a result of stochastic clustering of these energy deposits or radical attacks. A similar approach has been used in the CA simulations by Holley et al. [22]. The other existing CA models have taken DSB

as their starting point, and distributed them randomly (yet considering amorphous track structure for high-LET radiation) over the simplified DNA structure models.

The DSB repair module in PARTRAC uses a fully kinetic model. The attachment, action and detachment of core repair proteins of the NHEJ pathway are traced, as well as the spatial movement of the DNA ends. The parameters for this model have been derived from enzyme attachment, DSB repair kinetics, and chromatin dynamics data. Assessment of CA yields and kinetics comes as a by-product of DSB repair simulations, in the sense that not a single parameter has been adjusted to the analyzed CA data. Contrary to this approach, the previous CA models consider only the outcome of the repair process, without representing its kinetics. Movement of DNA ends is not followed in such models, and ad hoc assumptions have to be made on which ends may join at all and how likely misrejoining is as compared to proper joining: Chromosome ends within 1 μm distance are assumed equally likely to join in the CA model by Ballarini et al. [7,8,20,21], and a Gaussian distance dependence with mean range of joining of 0.9 μm is assumed by Ponomarev et al. [25]. The present simulations provide methods that may guide the choice of distance-dependent misrejoining probability, and indicate that such long-range interactions between chromosome ends are quite rare (Fig. 6).

Taken together, the PARTRAC family provides a unique modelling framework for track structure, DNA damage, repair and CA kinetics. This systems approach integrates the results of a number of theories and models of processes underlying the biological effects of radiation, among them radiation interaction with matter (cross sections), radiation chemistry (formation of reactive species, their diffusion and mutual reactions), DNA damage (by both direct energy deposits and radical attacks), and the repair of DSB via NHEJ. Individual steps have been thoroughly benchmarked against corresponding experimental data, as reviewed in [37].

The detailed mechanistic nature of the PARTRAC suite implies, however, that the models employ a relatively high number of parameters, which should be known for each cell line and conditions to be simulated. Variations among cell lines in their repair capacities, for instance, are likely responsible for their different radiation sensitivities in terms of cell killing. In the present work, we have used the simplifying assumption that the NHEJ repair in the AG1522 primary human skin fibroblasts under the experimental conditions used by Cornforth et al. [38] corresponds to that of the GM5758 fibroblast cells as determined in the experiments and protocols by Stenerlöw et al. [49], from which the parameters of the NHEJ repair module have been derived [35]. This assumption likely represents an oversimplification, but has been used because detailed information on the repair kinetics of the AG1522 fibroblasts under the given conditions was not available. Computational expensiveness represents an issue related to the mechanistic nature of the model and the involvement of many processes and parameters. Thanks to the modular structure of PARTRAC, the simulations of CA kinetics do not start from scratch but use previous simulations of radiation tracks, DNA and chromatin structure, and DNA damage. Yet, simulating DSB rejoining and CA production over an experimental interval of 1 day, for instance, takes several hours of computation time on a high-end linux PC. Largely due to computational expensiveness issues, the simulations presented in this work have been performed with a single nuclear architecture only, although alternative configurations of DNA and chromosomes in the nucleus have been generated and are available. In particular, an analysis of CA involving given specific pairs of chromosomes (e.g. chromosome number 4 and 18) has to take into account the variation in chromosome structures among individual cells within a culture, as done by Kreth et al. [23].

The inclusion of heterochromatic and euchromatic regions in the DNA model is the first step towards a comprehensive consideration of this aspect of the genome structure in the framework of radiation-induced DNA damage and its processing. Further steps shall include benchmarking of initial DNA damage and testing of mechanistic descriptions of the impact of hetero- and euchromatic regions on the spatial and temporal dynamics of DNA repair in view of recent experimental studies [60]. However, these steps go far beyond the scope of the present work.

Some processes underlying the NHEJ repair and CA formation have been approximated and/or are not fully known at present. This concerns for instance the DSB 'opening' and chromatin remodelling step, assumed to occur before the attachment of Ku70/80, where experimental details and its likely dependence on the chromatin structure (euchromatin vs. heterochromatin) are not known in sufficient detail. The fast nature of this process, assumed in this work, is however indicated by the fast recruitment of Ku70/80 reported in enzyme attachment data [47,48].

The nuclear dynamics, a key component of CA kinetics, is in this work accounted for in a simplified way only. The multi-scale model of DNA and chromosome structure described in Section 2 is not implemented in a dynamic but in a static way only. Simulating the movement of DNA ends is not based on this detailed model, but assumes a semi-free diffusion, i.e. free diffusion limited by nuclear attachment sites, with significantly reduced diffusion for DNA ends in synapsis. This concept effectively provides sub-diffusive motion indicated in recent data on the mobility of undamaged and damaged chromatin and telomeres [53–55]. Nevertheless, the discrepancy between the simulations and experimental data on the absolute yields of dicentrics may point to having actually overestimated the break end mobility in the simulations. Sub-diffusive mobility tends to penalize large-scale movements as compared with free diffusion. An explicit assumption that DNA ends from DSB move sub-diffusively, e.g. due to the dense nature of the chromatin fibre network, would thus enhance proper rejoining (i.e. ligation of original partners) and reduce misrejoining and CA yields, including dicentrics. Furthermore, the two DNA ends from a DSB may be tethered by residual interactions with histones before these are released in the chromatin remodelling step or by enzymes such as the MRN complex [1,61]. Such phenomena would help hold the right partners together until a synaptic complex is made under the action of Ku/DNA-PKcs. If (sub-)diffusion of DNA ends had to compete with their tethering, the fraction of ends diffusing relatively far away would be considerably reduced, and hence the yields of CA and dicentrics decreased. The framework of the NHEJ and CA simulations in PARTRAC offers well-suited tools for detailed testing of such hypotheses; nevertheless, such testing exceeds the scope of the present paper.

Finally, note that the present PARTRAC model of CA formation in G0/G1 cell cycle phase attributes all CA to classical, DNA-PK-dependent NHEJ, the major DSB repair pathway in this phase. Alternative DNA-PK-independent pathways [1] have not been modelled explicitly; they may be considered as implicitly included as far as the underlying kinetics and spatial aspects are similar to the classical NHEJ. Naturally, the modelling presupposition that all CA could be traced to NHEJ shall be refined to account for the role of other repair pathways especially when extending the simulations to CA in cells irradiated in G2/S phase [2].

5. Conclusion

An extension of the PARTRAC biophysical simulation tool to account for the yields and kinetics of chromosome aberrations by radiation has been presented. Although the predicted induction of dicentrics after low dose γ-ray and α-particle irradiation are in absolute terms 2- to 5-fold higher than the measured ones, the shape of the dose-dependence agrees with the experimental results

for both radiation qualities. Simplifications in the model have been discussed that may contribute to this overestimation. In spite of these simplifying assumptions, the PARTRAC suite with the present model of CA induction during the course of NHEJ repair provides a suitable framework for a mechanistic representation of basic processes in cell nuclei in response to radiation insult and for testing specific quantitative hypotheses on the underlying processes. The present work significantly contributes to extending the applicability of PARTRAC simulations and their predictive power towards late radiation-induced endpoints. Further work in this direction shall address radiation-induced cell inactivation (cell killing), thus covering a key endpoint relevant to both radiation therapy and radiation risk assessment.

Conflict of interest

The authors declare that there is no conflict of interest.

Acknowledgement

This work has partially been supported by the German Federal Ministry for the Environment, Nature Conservation and Nuclear Safety (Funding Ref. No. SR/StSch/INT 3610S30015).

References

[1] L.H. Thompson, Recognition, signaling, and repair of DNA double-strand breaks produced by ionizing radiation in mammalian cells: the molecular choreography, Mutat. Res. 751 (2012) 158–246.
[2] H. Nagasawa, J.R. Brogan, Y. Peng, J.B. Little, J.S. Bedford, Some unsolved problems and unresolved issues in radiation cytogenetics: a review and new data on roles of homologous recombination and non-homologous end joining, Mutat. Res. 701 (2010) 12–22.
[3] M. Hada, H. Wu, F.A. Cucinotta, mBAND analysis for high- and low-LET radiation-induced chromosome aberrations: a review, Mutat. Res. 711 (2011) 187–192.
[4] G.I. Terzoudi, V.I. Hatzi, C. Donta-Bakoyianni, G.E. Pantelias, Chromatin dynamics during cell cycle mediate conversion of DNA damage into chromatid breaks and affect formation of chromosomal aberrations: biological and clinical significance, Mutat. Res. 711 (2011) 174–186.
[5] M.N. Cornforth, J.S. Bedford, A quantitative comparison of potentially lethal damage repair and the rejoining of interphase chromosome breaks in low passage normal human fibroblasts, Radiat. Res. 111 (1987) 385–405.
[6] R.K. Sachs, P. Hahnfeld, D.J. Brenner, The link between low-LET dose-response relations and the underlying kinetics of damage production/repair/misrepair, Int. J. Radiat. Biol. 72 (1997) 351–374.
[7] F. Ballarini, M. Merzagora, F. Monforti, M. Durante, G. Gialanella, G.F. Grossi, M. Pugliese, A. Ottolenghi, Chromosome aberrations induced by light ions: Monte Carlo simulations based on a mechanistic model, Int. J. Radiat. Biol. 75 (1999) 35–46.
[8] F. Ballarini, From DNA radiation damage to cell death: theoretical approaches, J. Nucleic Acids (2010) 350608, http://dx.doi.org/10.4061/2010/350608.
[9] E.J. Hall, A.J. Giaccia, Radiobiology for the Radiologist, seventh ed., Lippincott Williams & Wilkins, Philadelphia, 2012.
[10] K.K. Khanna, S.P. Jackson, DNA double-strand breaks: signaling, repair and the cancer connection, Nat. Genet. 27 (2001) 247–254.
[11] T.R. Kasparek, T.C. Humphrey, DNA double-strand break repair pathways, chromosomal rearrangements and cancer, Semin. Cell Dev. Biol. 22 (2011) 886–897.
[12] L. Hlatky, R.K. Sachs, M. Vazquez, M.N. Cornforth, Radiation-induced chromosome aberrations: insights gained from biophysical modelling, Bioessays 24 (2002) 714–723.
[13] M.S. Sasaki, Advances in the biophysical and molecular bases of radiation cytogenetics, Int. J. Radiat. Biol. 85 (2009) 26–47.
[14] A.T. Natarajan, Chromosome aberrations: past, present and future, Mutat. Res. 504 (2002) 3–16.
[15] A.A. Edwards, V.V. Moiseenko, H. Nikjoo, Modelling of DNA breaks and the formation of chromosome aberrations, Int. J. Radiat. Biol. 66 (1994) 633–637.
[16] V.V. Moiseenko, A.A. Edwards, H. Nikjoo, Modelling the kinetics of chromosome exchange formation in human cells exposed to ionising radiation, Radiat. Environ. Biophys. 35 (1996) 31–35.
[17] R.K. Sachs, D.J. Brenner, A.M. Chen, P. Hahnfeldt, L.R. Hlatky, Intra-arm and inter-arm chromosome intrachanges: tools for probing the geometry and dynamics of chromatin, Radiat. Res. 148 (1997) 330–340.
[18] R.K. Sachs, D. Levy, A.M. Chen, P.J. Simpson, M.N. Cornforth, E.A. Ingerman, P. Hahnfeldt, L.R. Hlatky, Random breakage and reunion chromosome aberration formation model; an interaction-distance version based on chromatin geometry, Int. J. Radiat. Biol. 76 (2000) 1579–1588.
[19] F.A. Cucinotta, H. Nikjoo, P. O'Neill, D.T. Goodhead, Kinetics of DSB rejoining and formation of simple chromosome exchange aberrations, Int. J. Radiat. Biol. 76 (2000) 1463–1474.
[20] F. Ballarini, A. Ottolenghi, Models of chromosome aberration induction: an example based on radiation track structure, Cytogenet. Genome Res. 104 (2004) 149–156.
[21] F. Ballarini, A. Ottolenghi, A model of chromosome aberration induction: applications to space research, Radiat. Res. 164 (2005) 567–570.
[22] W.R. Holley, I.S. Mian, S.J. Park, B. Rydberg, A. Chatterjee, A model for interphase chromosomes and evaluation of radiation-induced aberrations, Radiat. Res. 158 (2002) 568–580.
[23] G. Kreth, S.K. Pazhanisamy, M. Hausmann, C. Cremer, Cell type-specific quantitative predictions of radiation-induced chromosome aberrations: a computer model approach, Radiat. Res. 167 (2007) 515–525.
[24] Y.A. Eidelman, S.V. Slanina, I.V. Salnikov, S.G. Andreev, Mechanistic modelling allows to assess pathways of DNA lesion interactions underlying chromosome aberration formation, Russ. J. Genet. 48 (2012) 1247–1256.
[25] A.L. Ponomarev, K. George, F.A. Cucinotta, Computational model of chromosome aberration yield induced by high- and low-LET radiation exposures, Radiat. Res. 177 (2012) 727–737.
[26] P. Pfeiffer, W. Goedecke, S. Kuhfittig-Kulle, G. Obe, Pathways of DNA double-strand break repair and their impact on the prevention and formation of chromosomal aberrations, Cytogenet. Genome Res. 104 (2004) 7–13.
[27] F.A. Cucinotta, J.M. Pluth, J.A. Anderson, J.V. Harper, P. O'Neill, Biochemical kinetics model of DSB repair and induction of gamma-H2AX foci by non-homologous end joining, Radiat. Res. 169 (2008) 214–222.
[28] Y. Li, H. Qian, Y. Wang, F.A. Cucinotta, A stochastic model of DNA fragments rejoining, PLoS ONE 7 (2012) e44293, http://dx.doi.org/10.1371/journal.pone.0044293.
[29] R. Taleei, H. Nikjoo, Repair of the double-strand breaks induced by low energy electrons: a modelling approach, Int. J. Radiat. Biol. 88 (2012) 948–953.
[30] D. Dolan, G. Nelson, A. Zupanic, G. Smith, D. Shanley, Systems modelling of NHEJ reveals the importance of redox regulation of Ku70/80 in the dynamics of DNA damage foci, PLoS ONE 8 (2013) e55190, http://dx.doi.org/10.1371/journal.pone.0055190.
[31] L. Shi, P. Oberdoerffer, Chromatin dynamics in DNA double-strand break repair, Biochim. Biophys. Acta 1819 (2012) 811–819.
[32] M.J. Kruhlak, A. Celeste, G. Dellaire, O. Fernandez-Capetillo, W.G. Müller, J.G. McNally, D.P. Bazett-Jones, A. Nussenzweig, Changes in chromatin structure and mobility in living cells at sites of DNA double-strand breaks, J. Cell Biol. 172 (2006) 823–834.
[33] L. Ježková, M. Falk, I. Falková, M. Davídková, A. Bačíková, L. Stefančíková, J. Vachelová, A. Michaelidesová, E. Lukášová, A. Boreyko, E. Krasavin, S. Kozubek, Function of chromatin structure and dynamics in DNA damage, repair and misrepair: γ-rays and protons in action, Appl. Radiat. Isot. (2013), http://dx.doi.org/10.1016/j.apradiso.2013.01.022 [pii: S0969-8043(13)00023-7; Epub ahead of print].
[34] W. Friedland, P. Jacob, P. Kundrát, Stochastic simulation of DNA double-strand break repair by non-homologous end joining based on track structure calculations, Radiat. Res. 173 (2010) 677–688.
[35] W. Friedland, P. Jacob, P. Kundrát, Mechanistic simulation of radiation damage to DNA and its repair: on the track towards systems radiation biology modelling, Radiat. Prot. Dosim. 143 (2011) 542–548.
[36] W. Friedland, P. Kundrát, P. Jacob, Stochastic modelling of DSB repair after photon and ion irradiation, Int. J. Radiat. Biol. 88 (2012) 129–136.
[37] W. Friedland, M. Dingfelder, P. Kundrát, P. Jacob, Track structures, DNA targets and radiation effects in the biophysical Monte Carlo simulation code PARTRAC, Mutat. Res. 711 (2011) 28–40.
[38] M.N. Cornforth, S.M. Bailey, E.H. Goodwin, Dose responses for chromosome aberrations produced in noncycling primary human fibroblasts by alpha particles, and by gamma rays delivered at sublimiting low dose rates, Radiat. Res. 158 (2002) 43–53.
[39] D.E. Cullen, J.H. Hubbel, L. Kissel, EPDL97 The Evaluated Data Library, '97 Version, Lawrence Livermore National Laboratory, 1997.
[40] M. Dingfelder, D. Hantke, M. Inokuti, H.G. Paretzke, Electron inelastic scattering cross sections in liquid water, Radiat. Phys. Chem. 53 (1998) 1–18.
[41] M. Dingfelder, L.H. Toburen, H.G. Paretzke, An effective charge scaling model for ionization of partially dressed helium ions with liquid water, in: The Monte Carlo Method: Versatility Unbounded in a Dynamic Computing World, American Nuclear Society, La Grange Park, IL, 2005, ISBN 0-89448-695-0.
[42] M.S. Kreipl, W. Friedland, H.G. Paretzke, Time- and space-resolved Monte Carlo study of water radiolysis for photon, electron and ion irradiation, Radiat. Environ. Biophys. 48 (2009) 11–20.
[43] M.S. Kreipl, W. Friedland, H.G. Paretzke, Interaction of ion tracks in spatial and temporal proximity, Radiat. Environ. Biophys. 48 (2009) 349–359.
[44] G. Kreth, J. Finsterle, J. von Hase, M. Cremer, C. Cremer, Radial arrangement of chromosome territories in human cell nuclei: a computer model approach based on gene density indicates a probabilistic global positioning code, Biophys. J. 86 (2004) 2803–2812.
[45] M. Costantini, O. Clay, F. Auletta, G. Bernardi, An isochore map of human chromosomes, Genome Res. 16 (2006) 536–541.
[46] N.E. Morton, Parameters of the human genome, Proc. Natl. Acad. Sci. U. S. A. 88 (1991) 7474–7476.

[47] N. Uematsu, E. Weterings, K. Yano, K. Morotomi-Yano, B. Jakob, G. Taucher-Scholz, P.O. Mari, D.C. van Gent, B.P. Chen, D.J. Chen, Autophosphorylation of DNA-PKCS regulates its dynamics at DNA double-strand breaks, J. Cell Biol. 177 (2007) 219–229.
[48] A. Taghva, Y. Ma, M.R. Lieber, Analysis of the kinetic and equilibrium binding of Ku protein to DNA, J. Theor. Biol. 214 (2002) 85–97.
[49] B. Stenerlöw, E. Höglund, J. Carlsson, E. Blomquist, Rejoining of DNA fragments produced by radiations of different linear energy transfer, Int. J. Radiat. Biol. 76 (2000) 549–557.
[50] G.C. Smith, S.P. Jackson, The DNA-dependent protein kinase, Genes Dev. 13 (1999) 916–934.
[51] E. Riballo, L. Woodbine, T. Stiff, S.A. Walker, A.A. Goodarzi, P.A. Jeggo, XLF-Cernunnos promotes DNA ligase IV-XRCC4 re-adenylation following ligation, Nucleic Acids Res. 37 (2009) 482–492.
[52] I.M. Sokolov, Models of anomalous diffusion in crowded environments, Soft Matter 8 (2012) 9043–9052.
[53] I. Bronstein, Y. Israel, E. Kepten, S. Mai, Y. Shav-Tal, E. Barkai, Y. Garini, Transient anomalous diffusion of telomeres in the nucleus of mammalian cells, Phys. Rev. Lett. 103 (2009) 018102, http://dx.doi.org/10.1103/PhysRevLett.103.018102.
[54] T. Jegou, I. Chung, G. Heuvelman, M. Wachsmuth, S.M. Görisch, K.M. Greulich-Bode, P. Boukamp, P. Lichter, K. Rippe, Dynamics of telomeres and promyelocytic leukemia nuclear bodies in a telomerase-negative human cell line, Mol. Biol. Cell 20 (2009) 2070–2082.
[55] A. Bancaud, S. Huet, N. Daigle, J. Mozziconacci, J. Beaudouin, J. Ellenberg, Molecular crowding affects diffusion and binding of nuclear proteins in heterochromatin and reveals the fractal organization of chromatin, EMBO J. 28 (2009) 3785–3798.
[56] G. Du, G.A. Drexler, W. Friedland, C. Greubel, V. Hable, R. Krücken, A. Kugler, L. Tonelli, A.A. Friedl, G. Dollinger, Spatial dynamics of DNA damage response protein foci along the ion trajectory of high-LET particles, Radiat. Res. 176 (2011) 706–715.
[57] M.R. Lieber, The mechanism of double-strand DNA break repair by the nonhomologous DNA end-joining pathway, Annu. Rev. Biochem. 79 (2010) 181–211.
[58] R.B. West, M. Yaneva, M.R. Lieber, Productive and nonproductive complexes of Ku and DNA-dependent protein kinase at DNA termini, Mol. Cell. Biol. 18 (1998) 5908–5920.
[59] D. Alloni, A. Campa, M. Belli, G. Esposito, A. Facoetti, W. Friedland, M. Liotta, L. Mariotti, H.G. Paretzke, A. Ottolenghi, A Monte Carlo study of the radiation quality dependence of DNA fragmentation spectra, Radiat. Res. 173 (2010) 263–271.
[60] B. Jakob, J. Splinter, S. Conrad, K.O. Voss, D. Zink, M. Durante, M. Löbrich, G. Taucher-Scholz, DNA double-strand breaks in heterochromatin elicit fast repair protein recruitment, histone H2AX phosphorylation and relocation to euchromatin, Nucleic Acids Res. 39 (2011) 6489–6499.
[61] S.E. Lee, K. Myung, Faithful after break-up: suppression of chromosomal translocations, Cell. Mol. Life Sci. 66 (2009) 3149–3160.